DEPTH MIGRATION VELOCITY ANALYSIS BY VELOCITY CONTINUATION IN COMMON-IMAGE GATHERS

G. R. Gomes, J. Schleicher, A. Novais, and H. B. Santos

email: *grgneco@gmail.com, js@ime.unicamp.br*

keywords: *Migration velocity analysis, depth-migration, velocity model building, seismic velocity interpretation and processing*

ABSTRACT

Building depth velocity models are essential for better images that help to reduce the exploration risk. In this paper, we implement the image continuation technique in the Common Image Gather (CIG) domain for an application to depth migration. Through the concept of residual-moveout (RMO) analysis, we develop a rather inexpensive routine for velocity analysis. This migration-velocity-analysis (MVA) tool allows building velocity models to migrate in depth starting at an extremely simple initial velocity model. We demonstrate the method's ability to construct acceptable models in depth without the need for prior information. The results obtained for synthetic data corresponding to a three-layer model and the Marmousoft data demonstrate the method's potential of generating first migration velocity models in depth.

INTRODUCTION

Many authors have studied Migration Velocity Analysis (MVA) as a way to obtain or improve the migration velocity model. The methods discussed cover a range that begins with a simple comparison of common-offset images (Gardner et al., 1974), evolves into coherency evaluation of imaged traces after constant-velocity migration (Sattlegger, 1975), extrapolation of CMP families (Yilmaz and Chambers, 1984), tentative migrations followed by stacking (Fowler, 1985) and analysis of depth focusing (Jeannot et al., 1986) to culminate in the analysis of the residual moveout (RMO) within the Common Image Gather (CIG) in the common angle-domain (angle-domain CIG, ADCIG), as discussed by Biondi and Symes (2004).

Because of its conceptual clarity and simplicity (Zhu et al., 1998), RMO analysis has become a favourite tool for MVA. Based on the concept of velocity continuation (Goldin, 1994; Fomel, 1994, 1997, 2003), also called image-wave propagation (Hubral et al., 1996; Schleicher et al., 2004), Schleicher et al. (2008) constructed a tool for RMO analysis in the time-migrated offset-domain CIG. This MVA method makes use of a partial differential equation (PDE), referred to as image-wave equation, that describes the repositioning of an event in the CIG under variation of the migration velocity. The idea is to propagate the events inside a CIG as if they were conventional waves, however with different kinematics, until they align horizontally. In this way, for each identifiable event, one finds a value of the velocity that flattens it. After migration with the so-constructed model, the procedure can be iterated to improve it.

By means of a finite-difference implementation of this image-wave equation, Schleicher et al. (2008) demonstrated the use of this MVA method on the Marmousoft data (Billette et al., 2003). Starting the analysis at a simple constant initial velocity model, they were able to use the method to recover an acceptable velocity model for time migration of the Marmousoft data. Based on this experience, it is important to observe that the greatest asset of MVA by image propagation within a CIG is its ability to construct an image from a basic initial model. In this respect, this method differs fundamentally from tomographic or full waveform inversion methods, which require a good initial velocity model to guarantee convergence.

Unfortunately, although Schleicher et al. (2008) theoretically investigated the method in both the time and depth domains, they implemented and tested only the time-domain version. Time migration is only applicable in media with little lateral variation. Thus, the migrated image of the Marmousoft data is impaired in the central region, where there are faults and high lateral velocity variations.

In this work, we address the depth-domain version of image continuation in a CIG. We implemented and tested the corresponding EDP in depth. To update the velocity model during the iterations, we adapted the procedure of Santos et al. (2015) based on the numerical results of Schleicher et al. (2004) for depth velocity continuation. We apply the resulting depth MVA technique to synthetic data from a simple three-layer model and to the Marousoft data. Our results are encouraging. Starting at a constant-velocity model, already the first iteration is able to produce a reasonable model for depth migration. Such a model may later be refined with more sophisticated tomographic or MVA techniques.

METHODOLOGY

When migrating the same data with different velocity models, the reflector images end up at different positions in depth. In a common-image gather (CIG), this gives rise to differently shaped curved events. Schleicher et al. (2008) studied the kinematics of the dislocation of these events as a function of migration velocity and derived a partial differential equation which describes it in analogy to wave propagation. Starting at the expression which describes the migrated pseudo-depth of a horizontal reflector in a homogeneous medium (Al-Yahya, 1989; Schleicher and Biloti, 2007), they arrived at

$$\frac{\partial P}{\partial z} + \frac{vz}{h^2 + z^2}\frac{\partial P}{\partial v} = 0, \tag{1}$$

where P is the wavefield describing the event in the depth CIG, v is the migration velocity, h is the half-offset and z is the migrated pseudo-depth. Equation (1) has the mathematical form of a 1D one-way wave equation, where v plays the role of the time variable and $(h^2 + z^2)/vz$ plays the role of the propagation velocity.

We discretize equation (1) for a solution by finite differences (FD) in an analogous way to the analysis of Schleicher et al. (2008) for the time-domain version of this equation. The resulting FD scheme reads

$$P_k^{n+1} - \alpha_k \left(P_{k+1}^{n+1} - P_{k-1}^{n+1}\right) = P_k^n + \alpha_k \left(P_{k+1}^n - P_{k-1}^n\right) \ , \tag{2}$$

where $P_k^n = \tilde{u}(\tau_k, v_n)$ or $P_k^n = u(z_k, v_n)$ and

$$\alpha_k = \frac{\beta_k}{4}\left(\frac{\Delta v}{\Delta z}\right) \ , \tag{3}$$

with

$$\beta_k = \frac{h^2 + z_k^2}{\bar{v} z_k} \ . \tag{4}$$

The value $\bar{v}$ represents the migration velocity at the present step, calculated as its mean at $n + 1/2$, i.e., $\bar{v} = (v_{n+1} + v_n)/2$. As discussed in Schleicher et al. (2008), the amplification factor of the FD scheme (2) has unit modulus, which means that it is unconditionally stable.

Using the FD scheme, equation (2), it is possible to continue a CIG from a given starting velocity to the desired one. In the continuation, the initial reference velocity used for the propagation step is defined equal to the constant velocity that generated the CIG. Thus, starting from a CIG obtained by a migration with constant velocity one can determine the CIG at another velocity without having to migrate. The variation of the image in the CIG due to the change in velocity reflects in the moveout of the event curve. The event horizontalizes if the velocity reached by continuation is approximately equal to the correct velocity of the event. Otherwise, a moveout occurs. This type of analysis is known as RMO analysis. The image continuation in the CIG allows varying the moveout of the events in the CIG by varying velocity. Therefore, the objective is to detect horizontal events in the propagated image gathers in order to extract information of the associated depths and velocities. The model updating is achieved by attributing this updated velocity information to the corresponding lateral position and depth.

In order to do this, the average velocities at a certain depth need to be converted to interval velocities. The average velocity of the depth migration in the process of velocity continuation is described by the inverse of the average over the slowness (Schleicher et al., 2004). In this way, it is possible to convert the average velocities into intervals velocities. Assuming that the average velocities obtained for two events in z_j and z_{j+1}, below the depth z_0, are respectively V_m^j and V_m^{j+1}, the expression for interval velocity is

$$\frac{1}{V_r^j} = \frac{\left(\frac{z_j - z_0}{V_m^j} - \frac{z_{j-1} - z_0}{V_m^{j-1}}\right)}{(z_j - z_{j-1})}. \tag{5}$$

The obtained interval velocity generally contains an error associated with the determination of the average velocity because equation (1) is based on the horizontal layer model and a constant-velocity assumption. This error leads to residual moveout in the CIG after migration with the updated velocity model. In this case, a further improvement of the model is required.

The described continuation procedure can be iteratively applied to improve the model. However, in this case, the starting velocity is no longer constant. This imposes a problem to the procedure because equation (1) or its corresponding FD scheme (2) require a constant velocity value for the calculations. As in the time-domain version, the solution is to proceed with a constant reference velocity in the range of the velocity values observed in the model. By this trick, the velocity updates are no longer absolute velocity values, but become corrections that are relative to the chosen reference velocity.

In this work, we have tested two assumptions for the relationship between the relative and absolute velocity values. Let us denote two model velocity values for event j in two subsequent iterations i and $i+1$ by $V_{m,i}^j$ and $V_{m,i+1}^j$. Furthermore, assume that the reference velocity is represented as V_r and the average velocity value that flattened event j is given by V_f. Then, we have the following expressions for the model update. Assuming a velocity update, the model slowness at position n can be calculated as

$$\frac{1}{V_n} \approx \frac{1}{V_{m,i+1}^j} = \frac{1}{V_{m,i}^j + V_f^j - V_c}, \tag{6}$$

and assuming a slowness update, this value becomes

$$\frac{1}{V_n} \approx \frac{1}{V_{m,i+1}^j} = \frac{1}{V_{m,i}^j} + \frac{1}{V_f^j} - \frac{1}{V_r}. \tag{7}$$

The iterative process of constructing and updating the velocity model is similar to the time-domain version described in Schleicher et al. (2008). The workflow for the velocity model building consists of the following steps:

1. Migrate the data using any constant velocity and sort the data into CIGs.
2. Apply the continuation of certain CIGs.
3. Determine the velocities and depths which flattens the events in the CIGs.
4. Construct a new migration model using step (2). If it is the first run, just fill the model. Otherwise, for subsequent execution, it is necessary to update the velocity model using the expressions (3) or (4).
5. Migrate the data using this new velocity model.
6. Apply the continuation one more time if the events in the CIGs are not satisfactorily flattened.
7. Repeat steps 3-6 until the events in the CIGs are satisfactory flattened.

NUMERICAL EXAMPLES

We tested our new depth MVA by velocity continuation in CIGs by applying it to synthetic data sets from two different isotropic models. We start with a simple model with three layers above a homogeneous halfspace. Next, we applied the technique to the Marmousoft data set (Billette et al., 2003).

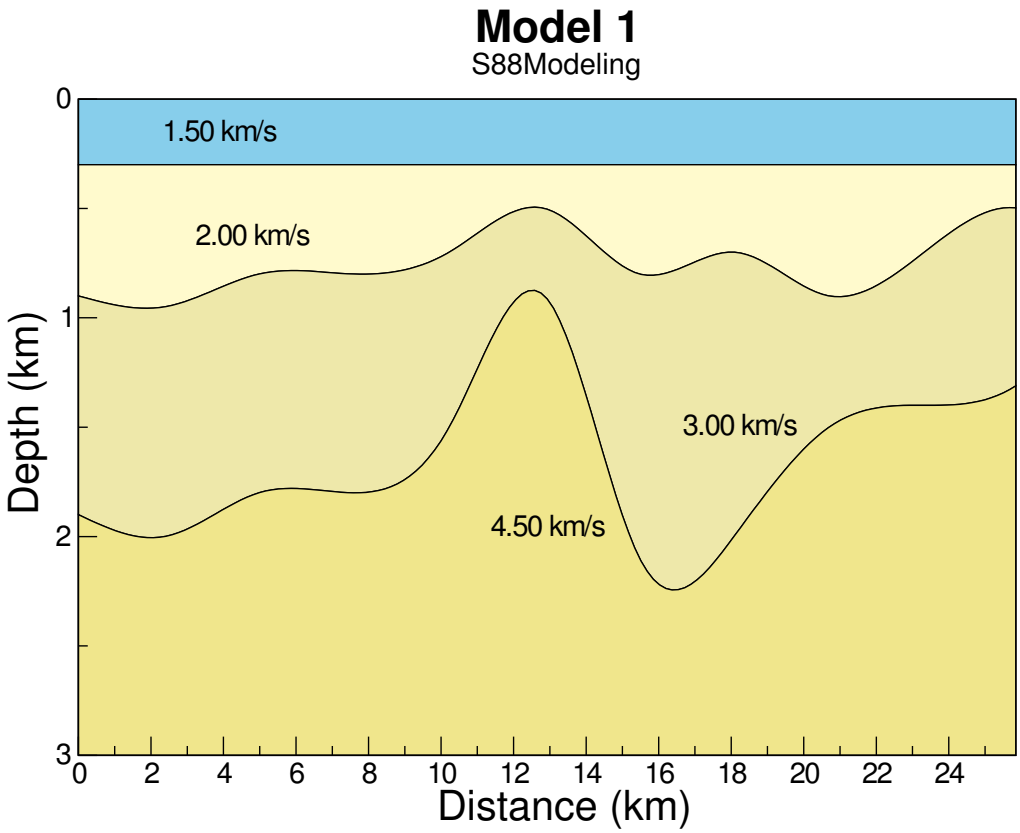

Figure 1: True velocity model with smooth interfaces to allow for ray tracing to generate synthetic data.

Three-layer model

Our first model consists of three homogeneous layers (Figure 1) above a homogeneous halfspace, separated by a horizontal and two smoothly curved interfaces. The true velocities in the model are, from top to bottom, 1500 m/s, 2000 m/s, 3000 m/s, and 4500 m/s. In this model, we generated a synthetic data set using the paraxial ray tracing of the SM88Modeling program implemented in the GêBR interface (Biloti, 2010). The data is regular and consists of 50 constant-offset sections, with a 100 m interval between sections, being the nearest-offset section the one for $h = 50$ m and the farthest one at $h = 4950$ m. The distance between the CMPs is 50 m.

We migrated the data with a constant velocity of 2000 m/s, according to step 1 of the velocity model building workflow. In accordance with step 2, we selected 51 CIGs at every 500 m to be continued to velocities ranging from 1400 m/s to 4000 m/s, with an initial velocity of 2000 m/s. The FD scheme was evaluated in steps of 1 m/s, saving snapshots at every 10 m/s. In these snapshots, we evaluated the semblance along horizontal lines. Figure 2 depicts the resulting semblance spectrum for the CIG at 7550 m.

In the velocity spectrum of Figure 2, as well as in the other 50 corresponding spectra, we manually picked the semblance peaks that defined the best values for depth and average velocity. From these picks, we then built the updated velocity model. As an example, Table 1 shows the picked depth and velocity values obtained in the velocity spectrum of CIG 7550 m, and Table 2 presents the resulting values of the velocity model as obtained according to equation 5. Also shown in Table 2 are the velocity errors with respect to the true model. Note that there is no information about the velocity of the lower halfspace in the data because no reflections occur below the deepest interface.

To fill in the overall model from the velocity profiles at the 51 selected CIG positions, we linearly interpolated the depth and velocity values between the positions. Figure 3 shows the resulting first velocity

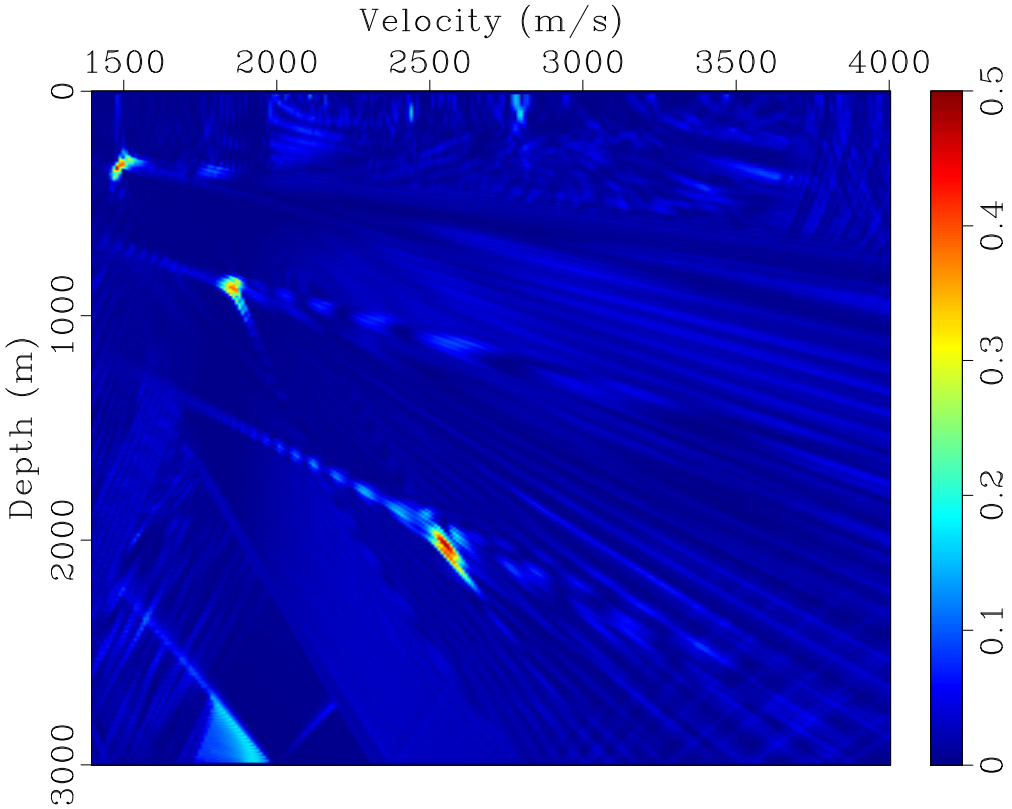

Figure 2: Velocity spectrum obtained after image-wave RMO correction by semblance calculation along horizontal lines in the continued CIG at 7550 m.

Table 1: Depth and average velocity values determined by picking the maxima in the semblance panel of Figure 2.

Depth (m)	Average velocity (m/s)
323.48	1498.31
902.61	1884.75
1961.74	2542.37

Table 2: Reflector depths and interval velocities calculated at the CIG at 7550 m from the picks (Table 1) in the semblance panel (Figure 2), and their respective relative errors.

Depth (m)	Error (%)	Velocity (m/s)	Error (%)
323.48	8	1498.31	-0.1
902.61	13	2201.97	10
1961.74	9	3618.27	20

model. Note that the velocity of the lower halfspace has been added for completeness, but was not obtained from the procedure. Also indicated in Figure 3 are the true positions of the three interfaces. We recognise that the general shape of the reflectors are already visible and the velocities are not too far off. Overall, we notice a shift towards higher velocities. The velocity errors are the largest where the reflector curvatures are the strongest. This was to be expected, because the theory was based on a planar-reflector assumption.

Since some velocity and depth values have relative error beyond 10% (Table 2) there is room for improvement. As a second step, we used this new velocity model of Figure 3 to migrate the data again, according to step 5 of the processing workflow. Figure 4 shows the resulting migrated CIGs. Although the most prominent features in these CIGs are the post-critical-angle artefacts, we recognise that the first event has been reasonably flattened, but that the other two events show some residual moveout. The frowns are consistent with our observation that the estimated velocities are too high. Therefore, we carried out two more iterations of the procedure.

Figure 5 compares the true velocity model (Figure 5a) with the estimated ones from all three iterations.

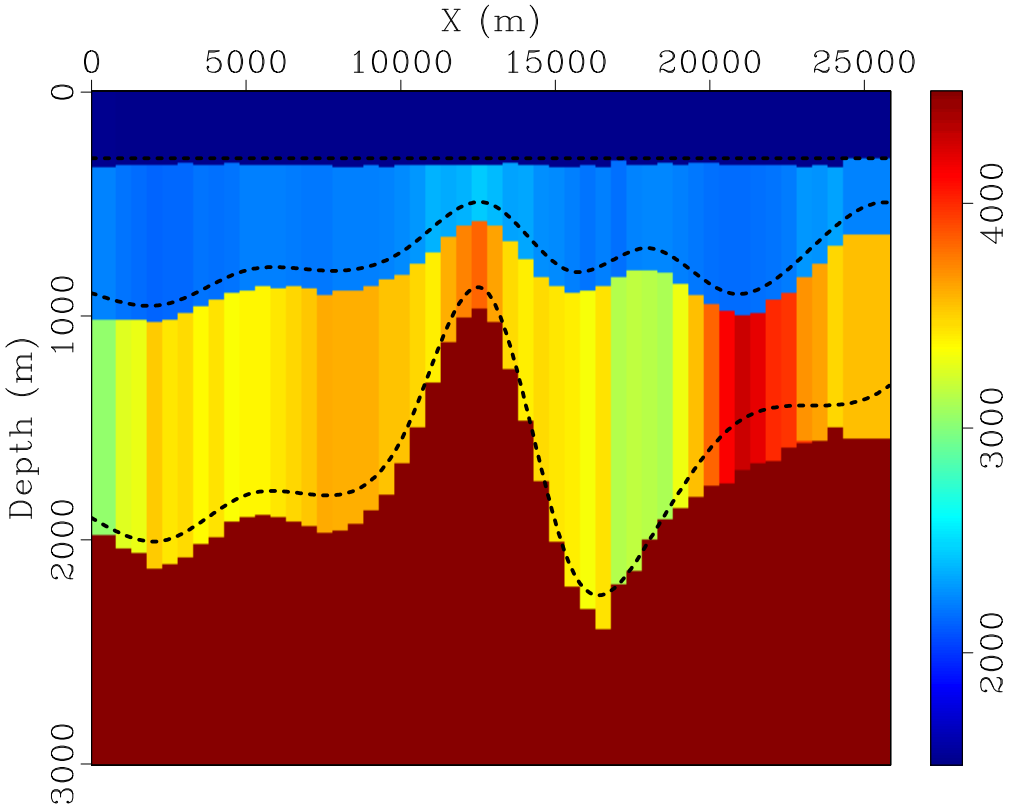

Figure 3: First inverted depth model.

In all iterations, we used a reference velocity of 2000 m/s. The procedure for velocity estimation and picking is the same as in the first iteration. Since the picked velocity values are now relative to the reference velocity, we updated the model velocities using formula (6).

Figure 5b, c, and d present the velocity models of the first, second, and third iterations, respectively. We see that the second iteration seems to lead to an overall improvement of the estimated velocity model, while the third iteration seems not to have gained much. Therefore, we stopped after the third iteration, recognising that the method presents convergence.

This convergence can also be observed in the CIGs. Figures 6 and 7 present the CIGs after the second and third iteration. We see that the second event is almost flat already after the second iteration (Figure 6) and the third event has considerably improved after the third iteration (Figure 7).

For the success and robustness of velocity model building, it is important to observe that the model convergence occurred in a top-down manner. This suggests to apply the technique using the layer-stripping strategy, correcting as much as possible the velocity in the shallower layers before attempting to flatten the deeper events. In this case, it is recommendable to keep the model fixed in the shallower, already processed part, so as to avoid unnecessary updating of the depth and velocity values for events that have already been acceptably flattened. Moreover, the reference velocity can then be chosen as the mean velocity for the present layer in the current iteration step, simplifying the updating procedure.

In another set of tests on this first model, we carried out the same procedure using the slowness-updating formula (7). We observed the same general behaviour as for the velocity-updating formula (6). However, convergence seemed to be a little bit slower.

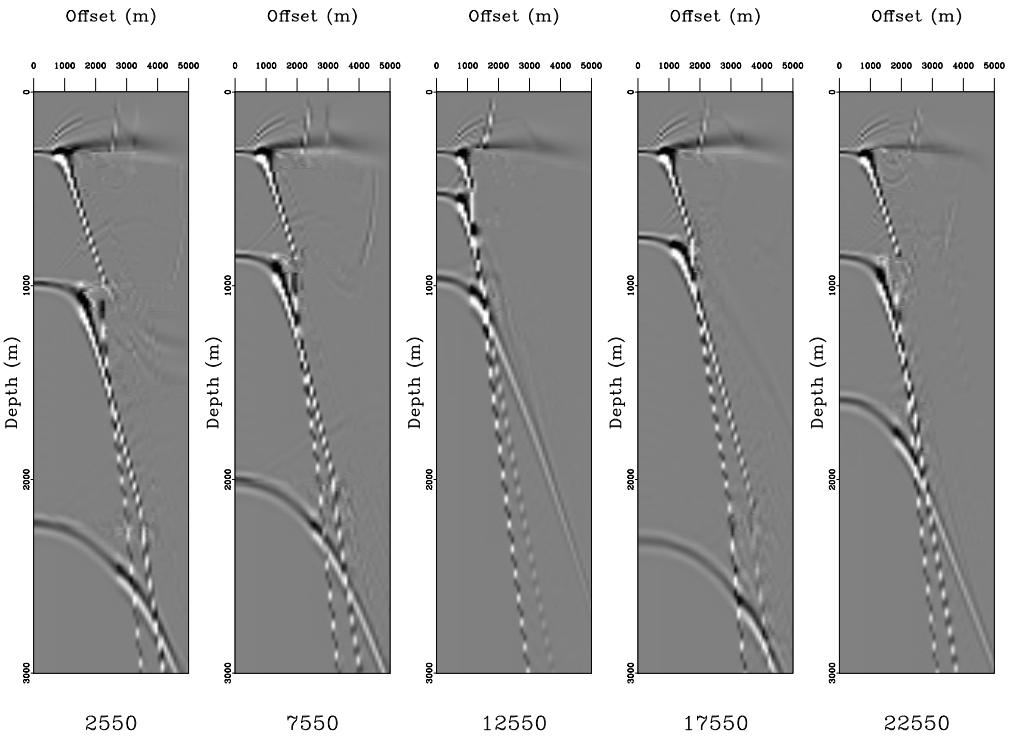

Figure 4: Selected CIGs after migration using the velocity model from the first iteration (Figure 3).

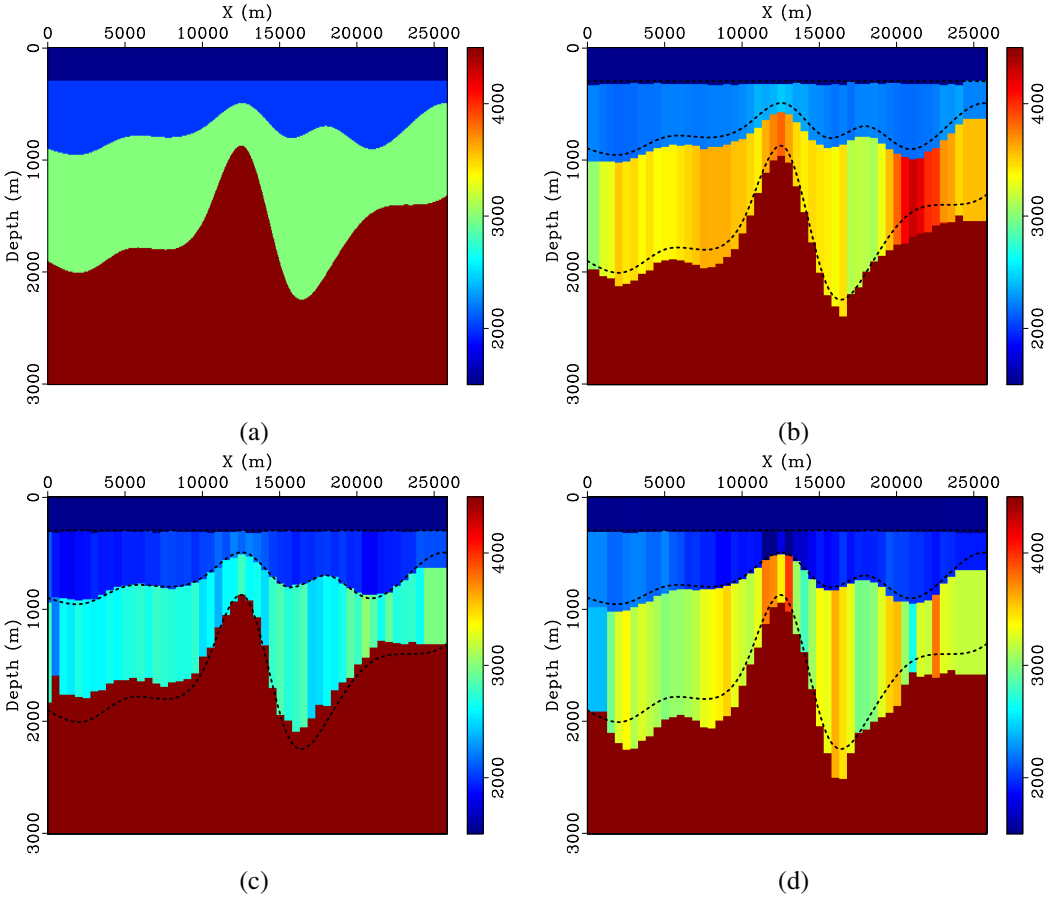

Figure 5: Evolution of velocity models after image continuation. (a) True model (a) and recovered model after one (b), two (c), and three (d) iterations. Model update according to expression 6. The dotted lines represent the real interfaces.

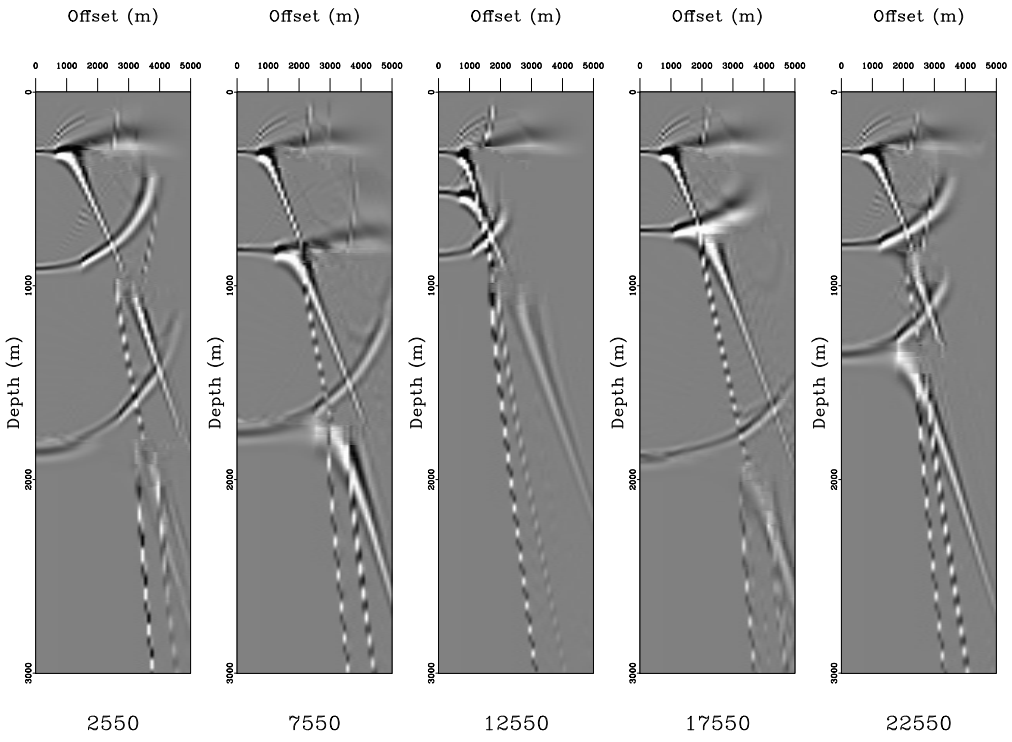

Figure 6: Selected CIGs after migration using the velocity model from the second iteration (Figure 5c).

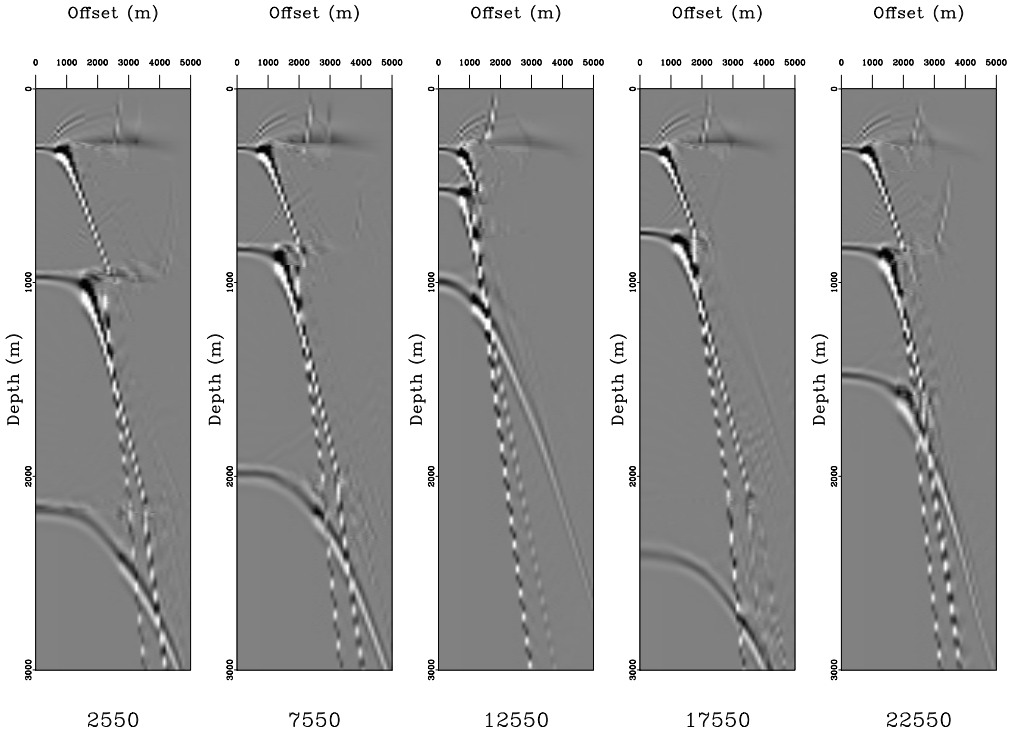

Figure 7: CIGs obtained after migration using the velocity model from the third iteration (Figure 5d).

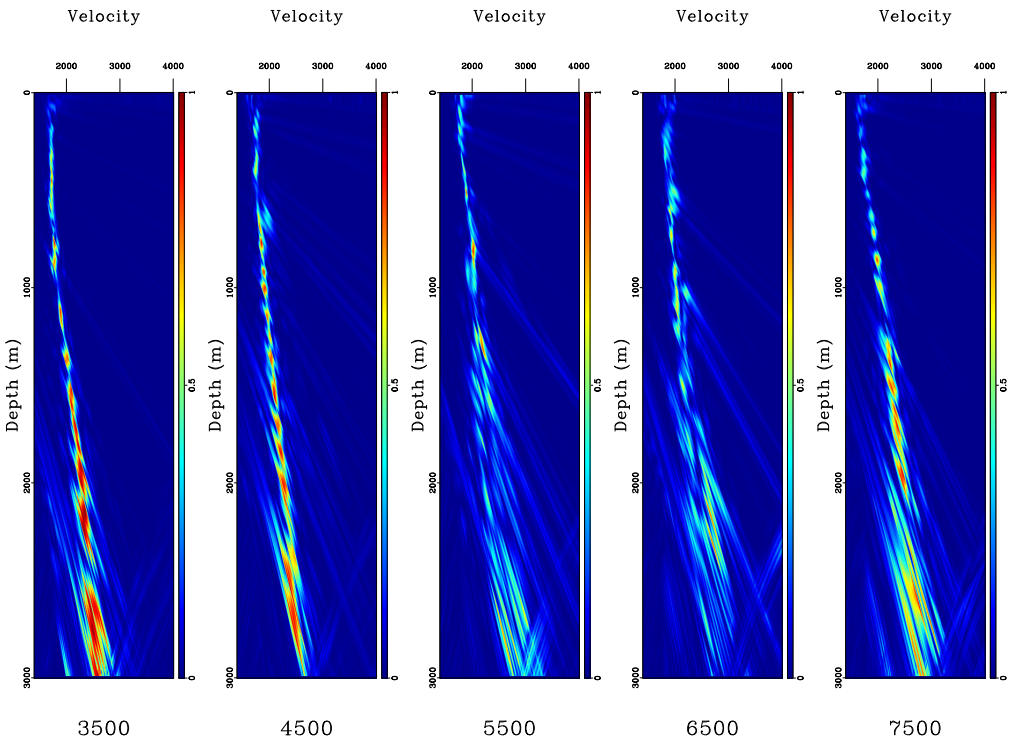

Figure 8: Selected velocity semblance spectra for the Marmousoft data.

Marmousoft model

For a somewhat more realistic test, we applied our MVA method to the Marmousoft data. These are synthetic data simulated by Born modeling using a smoothed version of the Marmousi model for wave propagation, but its original reflectivity for the secondary sources (Billette et al., 2003). The dataset consists of 96 constant-offset sections with a spacing of 25 m, the nearest one being at 100 m and the farthest at 2475 m. CMP spacing was and 12.5 m. We selected 35 CIGs at every 250 m to be continued. As for the first model, we used a velocity range from 1400 m/s to 4000 m/s with FD interval of 1 m/s and output at every 10 m/s. Again, we started with a constant-velocity migration using a reference velocity of 2000 m/s.

Figure 8 shows the resulting semblance sections at five CIG positions. The semblance panels in the CIGs at 5500 m and 6500 m, which are in the central part of the model, do not exhibit well-defined peaks below 1000 m depth as the others semblance panels. This happens due to the complexity of the medium in these areas, where a single average velocity is insufficient to describe the events. Moreover, the ambiguity in this areas increases the chances of errors during the model building process. However, after the first iterations, we found these areas of strong ambiguity do move down to deeper areas, reinforcing the idea of a layer-stripping application of the methodology.

Figure 9 shows the velocity model obtained with a single iteration only, and Figure 10 depicts the CIGs generated after migration using this model. Though the model does not allow to recognise the well-known Marmousi features, we find that the CIGs at the left-hand side of the model have been reasonably flattened in a single iteration. On the right-hand side, another iteration is required. This indicates that in simple geologic settings, the method should be capable of providing acceptable depth models with very few iterations.

In the centre part of the model, many events do not even present the expected curved shape. As mentioned above, this happens because a single average velocity is insufficient to describe them. However, we note that the shallow events have been improved over the constant-velocity migration, indicating that a layer-stripping strategy should be helpful to improve the velocity model in this area.

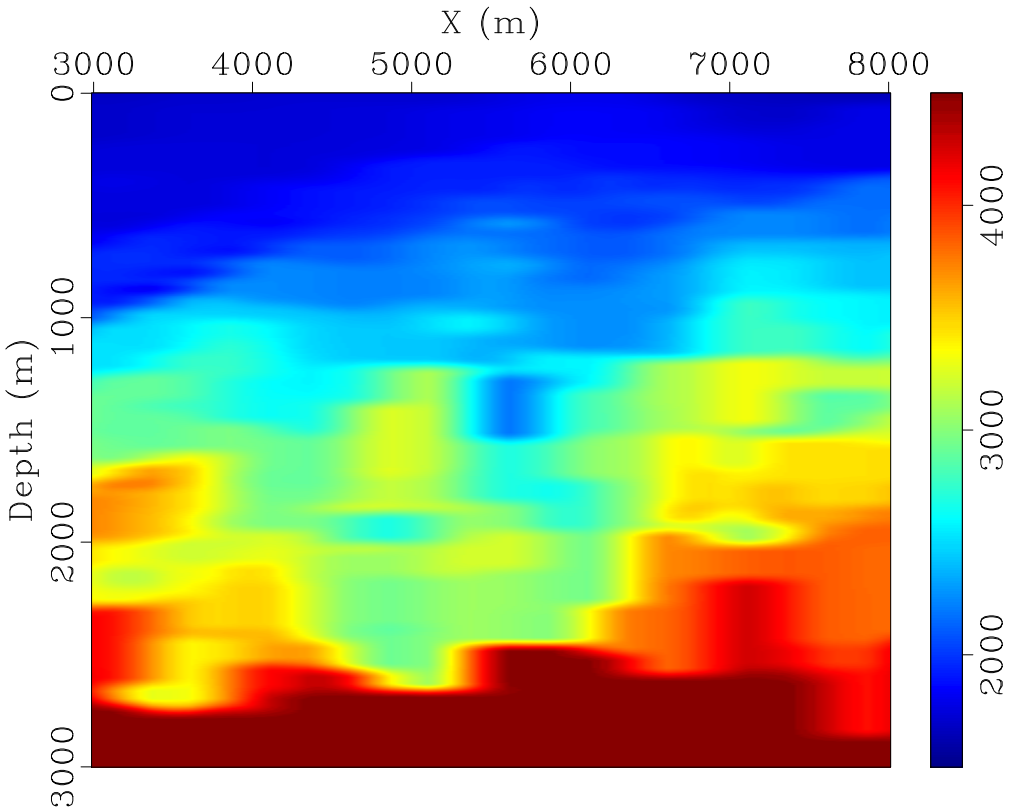

Figure 9: Velocity model from the Marmousoft data obtained with a single iteration of CIG continuation MVA.

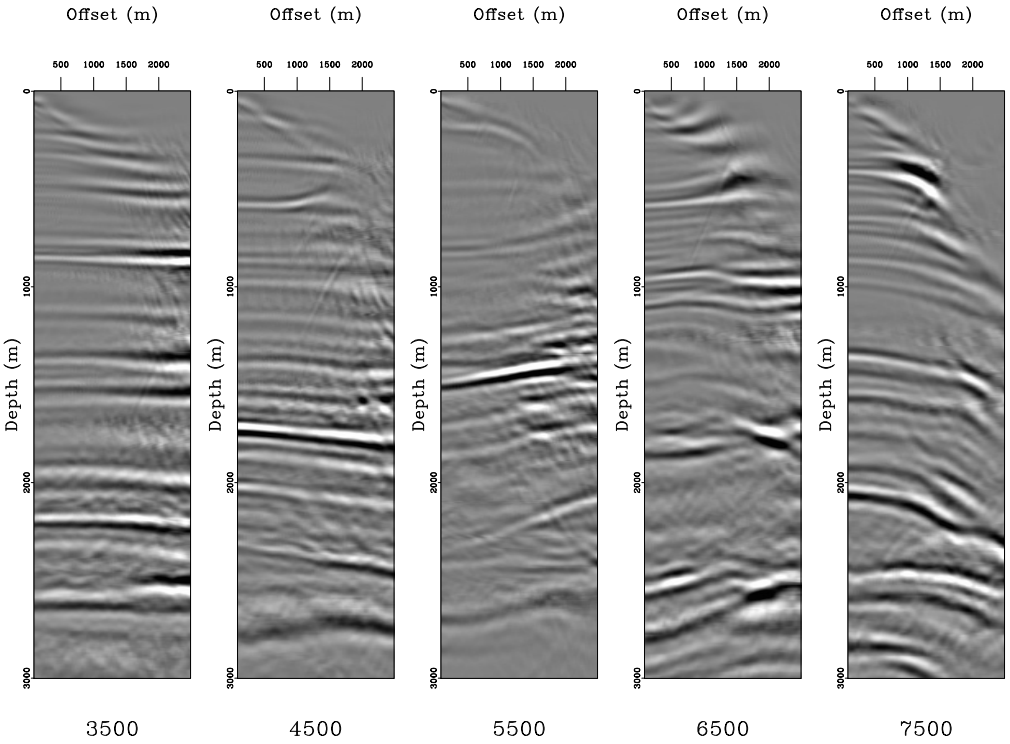

Figure 10: CIGs after migration of the Marmousoft data using the constructed velocity model after a single iteration (Figure 9).

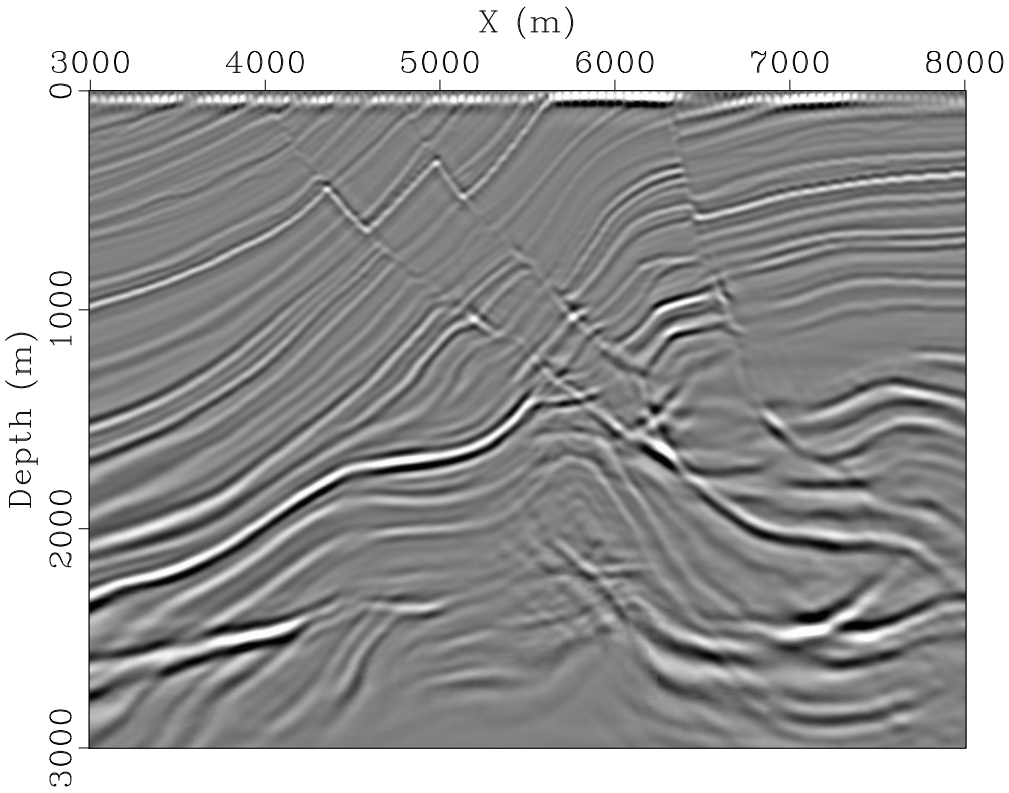

Figure 11: Depth migrated image (stacked) using the constructed velocity model after a single iteration (Figure 9).

Finally, Figure 11 depicts the stacked image of the corrected CIGS. The result shows that down to 2000 m the reflectors are well defined with all structures having been correctly positioned, and the faults are clearly visible and interpretable. However, in the central part of the model, particularly below 1500 m, the image is visibly distorted, presenting pull-up of events. Regardless, the method provided a good result already after a single iteration, demonstrating its promising potential.

CONCLUSION

In this work, we have developed a technique to depth-migration velocity model building using the image continuation of a CIG. The method uses a partial differential equation which describes the dislocation of a migrated event in a CIG as a function of migration velocity. Also, the method offers the possibility to update this first model to improve it through an iterative process. The method is rather inexpensive, because it simulates the results of multiple migrations with different migration velocities, reducing the need for an actual migration to once per iteration.

We have tested our new procedure on synthetic data corresponding to a model consisting of three layers above a homogeneous halfspace, and in a more sophisticated setting applied to the Marmousoft data. The technique presented promising results considering that in a first iteration, starting from a constant velocity model, it was already possible to obtain the morphology of the model we are inverting. This demonstrates its robustness with respect to an initial model.

Moreover, the test on the simple synthetic example has shown that the iterative process converges to a better model. Our results indicate that, though not employed here, a layer-stripping strategy should help to further improve the achievable model quality. In the case of the Marmousoft data, the obtained image (stacked section) from the first velocity model presents in a general way the correct structure of the model and highlights the faults.

ACKNOWLEDGMENTS

We thank Gilles Lambaré and Pascal Podvin for making the Marmousoft data set available to us. This work was kindly supported by Petrobras, the Brazilian national research agencies CAPES, CNPq, FAPESP, and FINEP. Henrique B. Santos is grateful to CGG-Brazil, Petrobras, ANP and PRH-PB230 for his fellowships. Additional support for the authors was provided by the sponsors of the *Wave Inversion Technology (WIT) Consortium*.

REFERENCES

Al-Yahya, K. M. (1989). Velocity analysis by iterative profile migration. *Geophysics*, 54(06):718–729.

Billette, F., Bégat, S. L., Podvin, P., and Lambaré, G. (2003). Practical aspects and applications of 2D stereotomography. *Geophysics*, 68(3):1008–1021.

Biloti, R. (2010). *S88 Modeling*. Department of Applied Mathematics, IMECC/UNICAMP. S88 Modeling employs Seis88 available in http://sw3d.mff.cuni.cz/ package developed by Vlatislav Cerveny and Ivan Psencik. Version 3. It is part of ToSCo Project.

Biondi, B. and Symes, W. W. (2004). Angle-domain common-image gathers for migration velocity analysis by wavefield-continuation imaging. *Geophysics*, 69(5):1283–1298.

Fomel, S. (1994). Method of velocity continuation in the problem of seismic time migration. *Russian Geology and Geophysics*, 35(5):100–111.

Fomel, S. (1997). Velocity continuation and the anatomy of residual prestack migration. In *Expanded Abstract, 67th Annual International Meeting*, volume II, pages 1762–1765, Tulsa. SEG.

Fomel, S. (2003). Time migration velocity analysis by velocity continuation. *Geophysics*, 68(5):1662–1672.

Fowler, P. (1985). Migration velocity analysis by optimization: Linear theory. *SEP Report*, 44:1–20.

Gardner, G. H., French, W. S., and Matzuk, T. (1974). Elements of migration and velocity analysis. *Geophysics*, 39(6):811–825.

Goldin, S. V. (1994). Superposition and continuation of transformations used in seismic migration. *Russian Geology and Geophysics*, 35(9):109–121.

Hubral, P., Tygel, M., and Schleicher, J. (1996). Seismic image waves. *Geophysical Journal International*, (125):431–442.

Jeannot, J. P., Faye, J. P., and Denelle, E. (1986). Pre-stack migration velocities from focusing depth analysis. In *Expanded Abstract, 56th Annual International Meeting of SEG*, pages 438–440, Houston, Texas. SEG.

Santos, H. B., Coimbra, T. A., Schleicher, J., and Novais, A. (2015). Prestack time-migration velocity analysis using remigration trajectories. *Geophysics*, 80(4):S151–S163.

Sattlegger, J. W. (1975). Migration velocity determination: Part I. philosophy. *Geophysics*, 40(1):1–5.

Schleicher, J. and Biloti, R. (2007). Dip correction for coherence-based time migration velocity analysis. *Geophysics*, 72(1):S41–S48.

Schleicher, J., Costa, J. C., and Novais, A. (2008). Time-migration velocity analysis by image-wave propagation of common-image gathers. *Geophysics*, 73(5):VE161–VE171.

Schleicher, J., Novais, A., and Munerato, F. P. (2004). Migration velocity analysis by depth image-wave remigration: first results. *Geophysical Prospecting*, 52(6):559–573.

Yilmaz, O. and Chambers, R. (1984). Migration velocity analysis by wave-field extrapolation. *Geophysics*, 49(10):1664–1674.

Zhu, J., Lines, L., and Gray, S. (1998). Smiles and frowns in migration/velocity analysis. *Geophysics*, 63(4):1200–1209.